Ab Initio Investigation of Charge Trapping Across the Crystalline-Si–Amorphous-SiO₂ Interface

Yue-Yang Liu,[1,2] Fan Zheng,[3] Xiangwei Jiang,[1,2,*] Jun-Wei Luo,[1,2] Shu-Shen Li,[1,2] and Lin-Wang Wang[3,†]

[1]*State Key Laboratory of Superlattices and Microstructures, Institute of Semiconductors, Chinese Academy of Sciences, Beijing 100083, China*

[2]*Center of Materials Science and Optoelectronics Engineering, University of Chinese Academy of Sciences, Beijing 100049, China*

[3]*Joint Center for Artificial Photosynthesis and Materials Science Division, Lawrence Berkeley National Laboratory, Berkeley, California 94720, USA*

Accurate microscopic description of the charge-trapping process from semiconductor to defects in the dielectric-oxide layer is of paramount importance for understanding many microelectronic devices such as complementary metal-oxide-semiconductor (CMOS) transistors, as well as electrochemical reactions. Unfortunately, most current microscopic descriptions of such processes are based on empirical models with parameters fitted to experimental device performance results or simplified approximations like the Wentzel-Kramers-Brillouin (WKB) method. Some critical questions are still unanswered, including: What controls the charge-hopping rate, the coupling strength between the defect level to semiconductor level, or the energy difference? How does the hopping rate decay with defect-semiconductor distance? What is the fluctuation of the defect level, especially in amorphous dielectrics? Many of these questions can be answered by *ab initio* calculations. However, to date, there are few *ab initio* studies for this problem mainly due to technical challenges from atomic-structure construction to large-system calculations. Here, using the latest advances in calculation methods and codes, we study the carrier-trapping problem using density-functional theory (DFT) based on the Heyd-Scuseria-Ernzerhof (HSE) exchange correlation functional. The valence bond random-switching method is used to construct the crystalline-Si–amorphous-SiO₂ (c-Si/a-SiO₂) interfacial atomic structure, and the HSE yields a band offset that agrees well with experiments. The hopping rate is calculated with the Marcus theory, and the hopping-rate dependences on the gate potential and defect distances are revealed, as well as the range of fluctuation results from amorphous structural variation. We also analyze the result with the simple WKB model and find a major difference in the description of the coupling constant decay with the defect-semiconductor distance. Our results provide the *ab initio* simulation insights for this important carrier-trapping process for device operation.

I. INTRODUCTION

Charge trapping at the gate dielectric layer along with the dangling-bond generation at the oxide-channel interface are known to be the main origins of electronic device reliability issues such as bias temperature instability (BTI) [1–10]. Such a charge-trapping and transport process is also important to the oxide protection layer in electrochemical cells. To date, the charge transport processes and the possible related ionic movements are often described by a continuous-diffusion equation (reaction-diffusion model) with physical pictures based on a simple effective mass such as the phenomenological model and parameters fitted to the experimental device's performance. However, it has recently been reported that the reaction-diffusion model [11–13] can fail to explain the BTI-degradation recovery [14–17], suggesting that charge trapping plays an important role in bias-temperature instability and a more realistic microscopic model might be needed [2,18–23]. Since charge-trapping processes are usually facilitated by the defect states in the gate oxide, great efforts have been made to understand the properties of these defects as well as the intrinsic electron trapping in SiO₂ and HfO₂ by using atomistic *ab initio* calculations [24–30]. In Ref. [24], Anderson et.al studied the precursors of low-energy E' centers in an ensemble of generated amorphous silica. In

_____

*xwjiang@semi.ac.cn
†lwwang@lbl.gov

Ref. [25], Kuo *et al.* investigated the structure and stability of surface oxygen vacancies in SiO$_2$, and found that structural interconversion is very likely to happen with thermal activation. El-Sayed *et al.* showed that the hydrogen-induced defects play a role in amorphous SiO$_2$ in Refs. [26] and [27], along with the intrinsic electron traps in amorphous SiO$_2$ in Ref. [28]. F. Cerbu *et al.* studied the intrinsic electron traps in amorphous HfO$_2$ in Ref. [29]. In Ref. [30], Mehes and Patterson constructed crystalline-Si–amorphous-SiO$_2$ [*c*-Si(001)/*a*-SiO$_2$] structures by using classical molecular dynamics simulation and studied the interfacial defects. In one of our previous works [31], we constructed the *c*-Si(001)/*a*-SiO$_2$ interface using the valence bond random-switching model and calculated the band alignment of such an interface using the Heyd-Scuseria-Ernzerhof (HSE) exchange-correlation functional. The HSE method allows us to yield accurate band gaps for both *c*-Si and *a*-SiO$_2$, and the calculated band offset for the interface agrees well with the experiments.

So far, *ab initio* calculations are used to study the single-defect level in *a*-SiO$_2$ and its variations, and are used to construct the *c*-Si(001)/*a*-SiO$_2$ interface. But there is no complete density functional theory (DFT) calculation yet for the charge trapping between the *c*-Si and the defects state in *a*-SiO$_2$. Several challenges might have prevented such calculations so far. First, in order to calculate the charge transfer, a large (e.g., 500 atoms) supercell needs to be used. That might be beyond the size regime one can calculate using the *ab initio* method. Second, in order to get the correct band gap and band alignment, computationally expensive methods, such as the HSE functional, need to be used. This makes the large supercell calculation even more difficult. Third, the charge-trapping rate is not so straight forward to calculate, especially to evaluate the electronic state coupling in such a disordered system. Finally, given the disordered nature of the amorphous structure, a systematic study (e.g., the trapping-rate-distance dependence) might be difficult. However, the charge-trapping-process calculation is critical. It will help us to provide the parameters in the phenomenological models and to understand the important trapping step in microscopic detail. Since it is unlikely that such microscopic processes can be precisely probed experimentally in the near future, realistic *ab initio* calculations of such processes become even more critical.

The charge-trapping process in a MOSFET manifests itself as a transfer of electrons and/or holes from the silicon channel to the oxide dielectric, which is a state-to-state transition from the silicon conduction- or valence-band state to the oxide-trap state. As far as we know, research on the charge-trapping process in MOSFETs has been largely contributed by Grasser *et al.* in Si/SiO$_2$ systems, by partially using DFT calculations, Wentzel-Kramers-Brillouin (WKB) approximation, and nonradiative multi-

phonon (NMP) theory [32]. The DFT calculation is used to obtain the eigenenergies of bulk Si and bulk SiO$_2$ separately instead of Si/SiO$_2$ interface structures given the computational capability and cost, and the WKB approximation is used to estimate the coupling constant between the initial and final states [20,32,33]

$$\theta_{ij} = \tilde{k} \exp\left(-\frac{\sqrt{2m_t \Delta V}}{\hbar}d\right), \tag{1}$$

where m_t is the tunneling mass, d is the distance from the *c*-Si/*a*-SiO$_2$ interface to the defect location, and ΔV is the tunneling barrier, which is usually taken as the conduction-band offset between the *c*-Si and *a*-SiO$_2$. $\tilde{k}$ is a prefactor fit to the experiment. Then the charge-trapping rate is calculated by the equation based on NMP theory

$$\tau_{i \to j}^{-1} = \frac{2\pi}{\hbar}|\theta_{ij}|^2 \sqrt{\frac{1}{4\pi k_B T}} \frac{1}{\sqrt{S\hbar\omega}}$$
$$\times \exp\left[-\frac{(E_j - E_i + S\hbar\omega)^2}{4S\hbar\omega k_B T}\right], \tag{2}$$

where E_i and E_j are the total energy of the system before and after charge trapping and $S\hbar\omega$ is the reorganization energy.

While these works are very pioneering and illuminating, it can be seen that the simulation framework is compromised by overlooking the effect of the Si/SiO$_2$ interface and estimating the coupling constant by WKB approximation instead of by accurate first-principle calculations. Furthermore, some critical parameters, such as the $\tilde{k}$, are not calculated. It will be better to consider the Si/SiO$_2$ interface explicitly because it can have a gradual change of band offset within a certain thickness near the interface, and there could be an issue of coupling between the *c*-Si electron state and the *a*-SiO$_2$ electron state. We also expect to improve the WKB description because there are several uncertainties concerning this formalism. First, what should one use for m_t and ΔV? If one considers this tunneling is from the *c*-Si CBM state, then perhaps the effective mass of *c*-Si should be used for m_t and the conduction-band minimum (CBM) band offset should be used for ΔV. On the other hand, if one considers this as the oxygen-vacancy (V_O) defect-state tunneling, perhaps the effective mass within *a*-SiO$_2$ needs to be used and a different ΔV needs to be used. It is also not clear whether a simple effective tunneling model can be used to describe the *a*-SiO$_2$ wave-function behavior. Finally, the $\tilde{k}$ has to be fit to the experiment, which significantly decreases the predictive power of the theory.

All of the above compromises can be overcome by direct *ab initio* calculations if the following tasks can be accomplished. First, a good atomic-structure model of

the c-Si/a-SiO$_2$ interface needs to be built. Second, the computational code should be fast enough to enable the calculation of large systems, especially using the HSE functional. The use of the HSE functional is critical to provide the correct band gap and band alignment between the c-Si and a-SiO$_2$ band edges, as well as the correct silicon CBM energy E_{CBM} and the oxide defect level E_{defect} levels. Third, a reliable procedure needs to be developed to calculate the electronic coupling constant and the related reorganization energy.

The first task can be accomplished by two different approaches: the molecular dynamics (MD) simulated annealing or covalent-bond-switching Monte Carlo simulation [31,34]. However, the time step for the MD simulation could be rather long, and the *ab initio* simulation of that process can be costly if no good classical force field can be used. We will thus use the covalent-bond random-switching method. The second task is difficult because the c-Si/a-SiO$_2$ atomic structure must consist of a large number (aproximately 500) of atoms to realistically represent the amorphous nature of the SiO$_2$. Fortunately, recent developments in computational algorithms and codes have made the direct calculation of systems with about 500 atoms feasible with the HSE functional. More specifically, using the plane-wave pseudopotential PWmat, which is implemented in graphics processing unit (GPU) [35,36], a 550-atom system can be calculated on an 8-GPU Mcluster within 6 h for a converged self-consistent field (SCF) calculation using the HSE-hybrid functional. The third task can be achieved by applying an electric field in the a-SiO$_2$ region to directly mimic the situation in the operation of a microelectronic device. When the electric field is large enough, the a-SiO$_2$ V_O defect level will cross the c-Si CBM level. Their energy anticrossing is directly related to their coupling constant. We also develop a technique, which inserts more of the a-SiO$_2$ layer between the defect and the c-Si without changing the local atomic environment of the V_O. This can significantly reduce the uncertainty due to V_O local environment fluctuation, while letting us focus on the distance dependence of the coupling constant.

After removing the above hurdles, all essential quantities needed to calculate the charge trapping can be obtained through the *ab initio* DFT method, and the charge-trapping rate can be calculated by the well-known Marcus charge transfer theory [37,38], which describes the electron transfer rate from an initial state to a final state as

$$\nu_{trapping} = \frac{2\pi}{\hbar} |V_C|^2 \sqrt{\frac{1}{4\pi\lambda k_B T}} \exp\left[-\frac{(\Delta G + \lambda)^2}{4\lambda k_B T}\right],$$

(3)

where V_C is the electronic coupling between the initial and final states and ΔG is the total Gibbs-free-energy difference between the initial (electron occupation configuration) atomic relaxed-ground state and the final (electron-occupation configuration) atomic relaxed-ground state. λ is the reorganization energy defined as the atomic relaxation energy after the electron reconfiguration from the initial state to the final state. The above formula is basically the same as Eq. (2), but with a more succinct form. The reorganization energy is represented as λ instead of $S\hbar\omega$ because it can be directly obtained by structural relaxation after hole trapping, and it is not necessary to calculate the phonon spectrum of the system. The V_C will also be obtained directly by DFT instead of by WKB approximation. Equation (3) has been successfully applied to semiconductor-molecule systems to study the electron- and hole-transfer dynamics [39,40]. Marcus theory is a classical limit formula for relatively high temperatures for systems with large degrees of freedom. It describes the multiphonon-energy transition with a classical thermodynamic limit. A quantum mechanical process can also be used to describe this phonon-energy-conservation process, and it has been shown that the difference is rather small for large systems [41]. Finally, a more rigorous treatment based on Franck-Condon approximation and static-state coupling can also be used to describe such a charge transport, in which all the electron-phonon-coupling constants and all the phonon modes of the system need to be calculated [42–44]. In this study, however, we will restrict ourselves to the Marcus theory as it describes the large system charge transfer well and it has a relatively simple computation procedure.

By constructing a set of c-Si/a-SiO$_2$ interfaces with approximately 500 atoms, and then using the plane-wave pseudopotential DFT code PWmat to conduct GPU-accelerated HSE functional-based DFT calculations, and finally studying the electron trapping rates with Marcus theory, we get the following discoveries: (1) The coupling constant between defect levels and Si CBM decays fast with the increase of defect-semiconductor distance, which is in accordance with the results of the WKB approximation. However, the coupling of these two energy levels might be more complicated than the scenario described by a simple one-dimensional (1D) WKB model. The coupling might be better described as the decays of the two wave functions toward each other and then meeting in the middle. If the WKB formalism is to be used, a more proper treatment is needed. First, the tunneling of both states must be taken into consideration and the Si CBM wave-function decays in a-SiO$_2$ might be more 1D, while the V_O wave function decays should be three-dimensional. This can end up with a more complicated distance-dependence formula. Second, the structural variety of a-SiO$_2$ results in a variation of the charge-trapping energy barrier and coupling constants, and further results in the charge-trapping-rate variation for the same defect. Third, the role of energy difference between the defect levels and CBM$_{Si}$ is more important than their coupling strength in deciding the

trapping rate when there is no bias. On the other hand, if a large electric field is applied, one asks what is the maximum possible charge transition rate during the scan of the electric field? Then the coupling constant will be the determining factor. Fourth, the oxygen vacancies alone inside the SiO$_2$ layer are rarely able to trap electrons under a small electric field, which is in agreement with previous works. Fifth, the DFT calculation is able to calibrate critical parameters for phenomenological models such as the WKB approximation in order to improve their accuracy and predictability.

This paper presents the *ab initio* calculations of the above-mentioned electron-trapping process at the *c*-Si and *a*-SiO$_2$ interface. It provides physical insights for the charge-trapping related reliability issues in complementary metal-oxide-semiconductor (CMOS) devices as well as the critical parameters for the phenomenological models used in device simulations. The remainder of the paper is organized as follows. The construction of the *c*-Si/-SiO$_2$ structures and the DFT calculation details are described in Sec. II. The calculated band alignment, reorganization energy, and coupling constant are shown in Sec. III. A comparison between the coupling constant calculated by the WKB approximation and DFT is discussed in Sec. IV. The calculated electron-trapping rates are presented in Sec. V. Section VI concludes the paper.

II. ATOMIC STRUCTURE CONSTRUCTION AND ELECTRONIC STRUCTURE CALCULATION

A. Atomic structure construction

As mentioned above, *a*-SiO$_2$ structures can be obtained by either MD simulations or bond-switching Monte Carlo (BSMC) simulations. It has been shown that the BSMC simulation reproduces the experimentally measured radial distribution function better than the MD simulation based on the ReaxFF model, and it also produces a more accurate O–Si–O angle-distribution function [31]. The BSMC simulation starts with a *c*-Si/*c*-SiO$_2$ heterostructure with several layers of *c*-Si and *c*-SiO$_2$ with a perfect bonding interface (although with a large strain in the SiO$_2$ region). Then a random pair of nearby Si–O bonds is selected (e.g., *A*–*B* and *C*–*D*) and switched into a new pair of bonds: *A*–*C* and *B*–*D*. Using a valence force-field model, which specifies which atom is bonded with which other atom, the new structure is relaxed, and its relaxed total energy is compared with the energy before bond switching. The new structure is then accepted or rejected following the Metropolis MC scheme. However, to make the structure amorphous, the first $N/2$ steps are all accepted (N is the number of atoms in the simulation cell). After that, a stimulated annealing process is carried out using the bond-switching process to cool the structure and to reduce the local strain. During this process, the *c*-Si side is kept unchanged by the bond-switching process.

The above process has been used in our previous work to generate the *c*-Si/*a*-SiO$_2$ interface, which yields the correct band offset across the interface [31]. However, the original *c*-Si/*a*-SiO$_2$ structures generated in Ref. [31] are periodic along the *x* direction perpendicular to the interface. Such a periodic structure is not suitable for investigating the electronic coupling between the *c*-Si CBM state and *a*-SiO$_2$ defect state since they can couple through both interfaces (at the left and right of the defect location). The periodic boundary condition is not consistent with a real MOSFET setup either. For these reasons, we have built a new structure with only one *c*-Si/*a*-SiO$_2$ interface, and open ends in the other *c*-Si interface and *a*-SiO$_2$ interface, as shown in Fig. 1. Such an open-ended structure can be obtained from the original periodic structure with a cut at one side and using pseudo-hydrogen atoms to passivate the cut surfaces. To generate the V_O defect, we simply remove one O from the *a*-SiO$_2$ side, and relax the system under DFT until the atomic forces become less than 0.02 eV/Å. The Perdew–Burke-Ernzerhof (PBE) functional is used for all structural relaxation while the HSE functional is used for energy-level calculations. The Si—Si bond at the oxygen vacancy is found to be 2.65 Å, which is much larger than that in bulk Si. Considering that such a nonperiodic system may increase concerns for the finite-size effects, we conduct a comparative study on the model shown in Fig. 1(a) with periodic and nonperiodic boundaries. Results show that the defect energy of
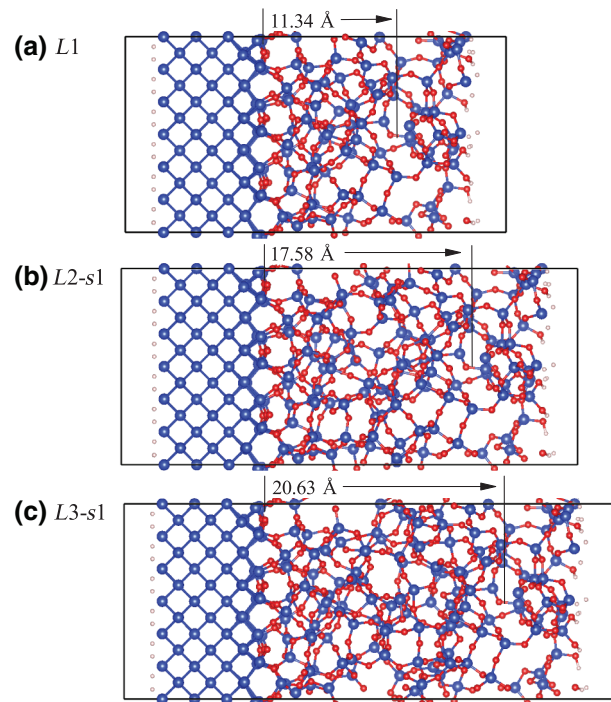
FIG. 1.   The *c*-Si/*a*-SiO$_2$ atomic structures studied in this work. The interface-defect distances are marked in each structure. Only two of the six elongated structures are presented here.

these two systems relative to the c-Si CBM differ by only 0.089 eV, which is much less than the fluctuation due to the different structure in the amorphous system, indicating that the finite-size effect is very small. In addition, all the models have a lattice of 16.3×16.3 Å^2 along the cross-section directions, and we have not seen strong coupling between the image defect states in the cross section of our model.

One of our goals is to investigate the effect of interface-defect distance ($d_{I\text{-}D}$) on the electron trapping. One can remove the O from a different location, thus changing the $d_{I\text{-}D}$. However, the V_{O}s constructed in that way will be different from one another. This will increase the uncertainty due to the variation of that defect. We like to keep the defect (oxygen vacancy) and the nearby atomic structure the same while changing the $d_{I\text{-}D}$. To realize that, we insert different layers of a-SiO$_2$ in a region between V_O and the interface. More specifically, we cut off one cross section between V_O and the interface, move these two pieces apart, and insert a slice of SiO$_2$ inside this region. This is followed by performing BSMC for the bonds inside this inserted slice, while keeping the other atoms fixed. After all this is done, a whole-system DFT relaxation is performed. In this way, we can keep the V_O local environment the same for different $d_{I\text{-}D}$ distances as shown in Fig. 1.

In addition to the $d_{I\text{-}D}$, we study the effect of structure variation in between the defects and the semiconductor, that is, by preparing three different inserting layers that vary in atomic structure, but with the same thickness. Consequently, seven models are investigated in this study, including one model with $d_{I\text{-}D} = 11.34$ Å, three models with $d_{I\text{-}D} = 17.58$ Å, and another three models with $d_{I\text{-}D} = 20.63$ Å. These models are denoted as $L1$, $L2$-$s1$, $L2$-$s2$, L2-$s3$, $L3$-$s1$, $L3$-$s2$, and $L3$-$s3$, respectively, where "L" denotes length and "s" denotes structure.

B. Electronic structure calculation

It is well known that the DFT calculation with the local-density approximation or generalized gradient approximation functional significantly underestimates the band gap of the semiconductors and does not yield correct energy levels. Such a problem is critical for studying the charge-trapping process because the trapping rate is closely related to the energy difference between the silicon band edge and the defect level. The energy level also affects the tunneling decay of the wave function, thus a simple scissor operator will not help. Consequently, extra care must be taken to ensure the correctness of the electronic structure and band alignment. This is challenging since the smallest c-Si/a-SiO$_2$ structure studied in this work contains 448 atoms and the largest one contains as many as 604 atoms. Here, we have used the PWmat package with the HSE-hybrid-functional calculation. The PWmat package is implemented with the GPU and can speed up the

calculation by 20 times compared to the CPU. Taking the H-passivated c-Si/a-SiO$_2$ structure with 550 atoms and 2550 electrons, for example, the HSE-functional-based SCF calculation takes only 6 h on 8 GPUs with SG15 norm-conserving pseudopotentials and an E_{cut} of 50 Ry. We confirm the validity of 50 Ry by repeating the SCF calculation on structure $L1$ with $E_{\text{cut}} = 60$ Ry and find no notable differences. Only the Γ point is sampled because the lattices and numbers of atoms in each model are so large. The validity of a single k point has been proven and shown in Sec. S1 of the Supplemental Material [45].

Another problem is that the c-Si/a-SiO$_2$ structures contain two regions of materials, one for c-Si and another for a-SiO$_2$. In order to yield an accurate band gap, it is necessary to fine tune the HSE Fock exchange-mixing parameter. Unfortunately, there is no single parameter that can yield accurate band gaps for both c-Si and a-SiO$_2$. Here, the PWmat package implements atom-weighted mixing parameters. More specifically, one can define a regional mask function as $f(r) = 1 + \sum_i a_i e^{-(r-R_i)^2/\sigma_i^2}$, where a_i and σ_i are atomic-type-dependent input parameters. With large σ_i, this function is smooth in space, but can have different values in different regions. The Fock exchange integral in the HSE total energy expression is then written as

$$\sum_{i,j} 0.25 o(i) o(j) \iint \psi_i(\mathbf{r}) \psi_j^*(\mathbf{r}) f(r) \frac{\text{erfc}[\omega(\mathbf{r} - \mathbf{r}')]}{|\mathbf{r} - \mathbf{r}'|}$$
$$\times f(r') \psi_i^*(\mathbf{r}') \psi_j(\mathbf{r}') d^3\mathbf{r} d^3\mathbf{r}',$$

where 0.25 is the default mixing parameter for HSE and $o(i)$, $o(j)$ are the orbital occupation numbers. Using a_i and σ_i as -0.1 and 4.2 for Si, and 0.24 and 2.75 for O, we get a c-Si band gap of 1.12 eV and a a-SiO$_2$ band gap of 8.5 eV, as measured by experiment. The calculated band offset between the CBM of c-Si and CBM of a-SiO$_2$ is 2.9 eV, in good agreement with the experimental results of 3.0 eV.

III. DFT CALCULATION RESULTS

The silicon band edge and the oxygen-vacancy defect levels in each structure are ascertained by checking the partial density of states (PDOS) of the crystalline Si part and the oxide defect part, respectively. Taking the shortest structure, $L1$, for instance, the PDOS is shown in Fig. 2(a). It can be seen that two defect levels are induced by the oxygen vacancy, including one level that lies above the Si conduction-band minimum (CBM$_{\text{Si}}$) and another one that lies below the Si valence band maximum. Such a phenomenon is in good agreement with previous works on a-SiO$_2$ [46]. Here, we study the electron-transfer process, which is most likely to happen from the silicon conduction band to the unoccupied defect level, thus we will focus on the CBM$_{\text{Si}}$ and the E_{defect} as marked in Fig. 2(a).
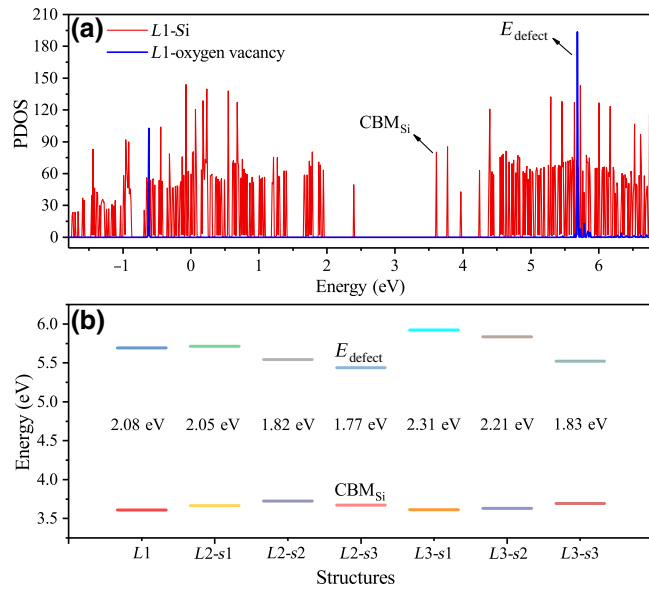
FIG. 2. The band alignment calculated by the HSE-functional-based DFT. (a) The partial density of states (PDOS) of the crystalline Si part and the oxygen-defect part. The PDOS of the defect is obtained by projecting the wave functions to the Si atoms close to the vacancy defect. The PDOS on c-Si is taken from the center of the c-Si slices. (b) The E_{CBM} and E_{defect} in different structures.

With the E_{CBM} and the E_{defect} known, it is tempting to use them to calculate the ΔG in the exponent of Eq. (3). However, it is worth pointing out that ΔG does not equal to $E_{defect} - E_{CBM}$. This is because E_{CBM} and E_{defect} are both obtained from the neutral structure, which will change when E_{CBM} or E_{defect} is occupied by an additional electron. Such a structural relaxation caused by electron occupation will result in a energy change of the system, which is called reorganization energy. The reorganization energy is calculated as follows: First, we relax the atomic structure with a defect at its neutral state (N electrons) and obtain an atomic structure R_0. We then place an additional electron in the R_0 structure ($N + 1$ electrons) and carry out an electronic structure self-consistent calculation to obtain the total energy $E(R_0, N + 1)$. After that, we relax the structure with $N + 1$ electrons to obtain its minimum energy $E(R_1, N + 1)$. The energy differences between these two atomic configurations (both with $N + 1$ electrons) is the reorganization energy

$$\lambda = E(R_0, N + 1) - E(R_1, N + 1). \tag{4}$$

Note that since both energies have $N + 1$ electrons, they both have electrostatic image energies, and thus should cancel each other out. The uncertainty caused by this image electrostatic interaction should be much smaller than the typical defect calculation where $E(N + 1)$ and $E(N)$ are subtracted. All of these calculations for reorganization energy are done using PBE.

Consider the original case when there are no electrons occupying the Si conduction band and the upper defect level, then the energy of the system can be denoted as E_0. Then we can write the Gibbs free energy before and after electron transfer as:

$$G_i = E_0 + E_{CBM} - \lambda_{CBM-Si}, \tag{5}$$

$$G_f = E_0 + E_{defect} - \lambda_{defect}. \tag{6}$$

Consequently,

$$\Delta G = E_{defect} - E_{CBM} - \lambda_{defect} + \lambda_{CBM-Si}. \tag{7}$$

It can be seen that E_{CBM} and E_{defect} are essential quantities that must be calculated first. Also, by analyzing the PDOS, the E_{CBM} and E_{defect} in other structures are obtained and are shown in Fig. 2(b). In Eq. (3), the total reorganization energy λ equals to the sum of λ_{defect} and λ_{CBM-Si}.

Due to the delocalization nature of the E_{CBM} state, the reorganization energy of the Si CBM state should be very small, thus it can be ignored. In contrast, the defect state is very localized, and the defect structure will respond strongly to the occupying electron. As seen in Fig. 3, in a V_O defect, the two Si atoms that are originally connected by the removed O atoms separate more from each other after the occupation of an electron, and the nearby atoms also move away slightly. The corresponding reorganization energy due to the occupation of the electron is calculated to be 0.68 eV.

The most important and difficult task is to calculate the coupling constant between the initial state (E_{CBM}) and the final state (E_{defect}). Our strategy is to apply an electric field to drive the two energy levels toward each other until the "anticrossing" occurs. Anticrossing, which is sometimes called "avoided crossing," is the phenomenon where two eigenvalues of a Hermitian matrix cannot become equal in value due to their electronic coupling. The energy difference minimum of the two eigenvalues is called the "anticrossing gap," which is equal to two times their coupling constant (V_C) [47,48]. Another approach to get the coupling constant is to use a linear combination of two relevant adiabatic states and then figure out the coupling constant by using the 2×2 Hamiltonian. The obtained coupling constant V_C is usually the same as that obtained from the avoided-crossing calculations [39,40]. See Sec. S2 in the Supplemental Material [45] for more discussion on this topic. The electric field is applied by changing the potential of each place along the Z direction. Denoting the potential of the system obtained by the HSE self-consistent calculation as $V_0(z)$ and the electric-field strength as $-F$, then by setting the center of the electric field at the Si/SiO$_2$ interface (z_0), we can create the new potential of the system as

$$V_{new}(z) = V_0(z) - F(z - z_0). \tag{8}$$
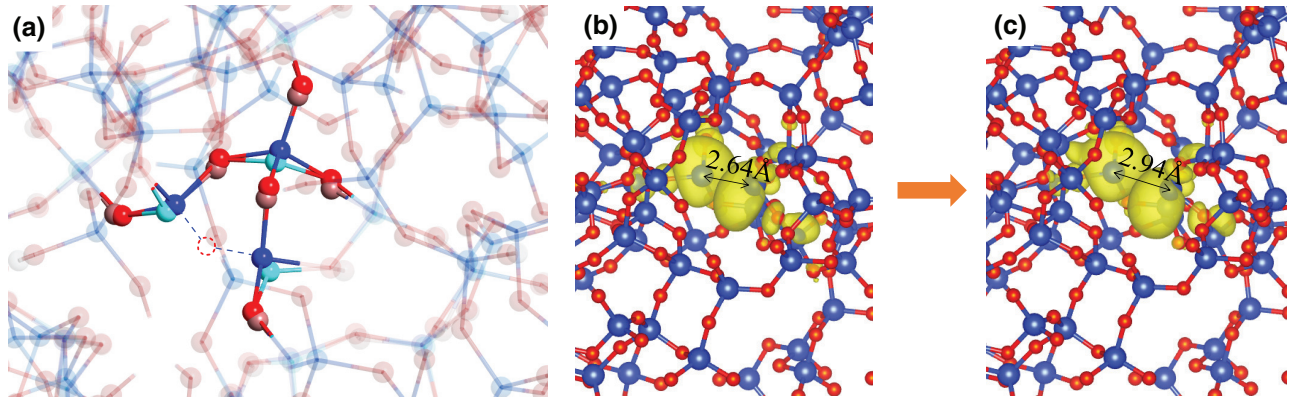
FIG. 3.   The structure reorganization of the oxygen-vacancy defect after trapping an electron. (a) The original Si and O atoms are denoted by dark blue and red, respectively. The Si and O atoms after reorganization are denoted by light blue and pink, respectively. The oxygen vacancy is denoted by a red dashed circle. (b),(c) The wave function of the defect level before and after reorganization.

Consequently, the energy levels in the Si part will rise and the defect level in the SiO$_2$ part will be pulled down. Taking structure $L1$ as an example, the transitions of E_{CBM} and E_{defect} and the corresponding wave functions are shown in Fig. 4. It can be seen that the wave function of E_{defect} is mainly localized at the oxygen-vacancy site before the coupling and the wave function of E_{CBM} is delocalized at the Si atoms. When the two energy levels approach each other, their wave functions begin to mix together with significant charge densities at both the defect and the crystalline Si sides for both wave functions. With a further increase of the electric field, the E_{defect} state continue to move downward while the E_{CBM} state moves upward and they become decoupled.

Although the coupling constant V_C is known to be half of the anticrossing energy gap [47,48] (the minimum of $E_{CBM}-E_{defect}$), challenges remain in order to yield a continuous curve of $E_{CBM}-E_{defect}$. To reduce the computational cost, we have fitted the energy curves with the eigenenergies of the following 2×2 model:

$$\det \begin{pmatrix} \eta(F - F_0) - E & V_C \\ V_C & -\eta(F - F_0) - E \end{pmatrix} = 0, \quad (9)$$

and thus

$$\Delta E = 2\sqrt{V_C^2 + \eta^2(F - F_0)^2}, \quad (10)$$

in which F is the applied electric field, $\Delta E = |E_{defect} - E_{CBM}|$, V_C, η, and F_0 are three unknown parameters, η roughly represents the distance between the defect state and the Si CBM state, and F_0 is the field amplitude of the crossing point. With this equation and five groups of calculated $(F, \Delta E)$ data, a fitted curve and V_C can be obtained. As is seen in Fig. 4(b), the fitted curve matches well with the calculated points and we get $V_C = 0.00188$ eV in this case. Note that this V_C is much smaller than the typical

accuracy of the DFT calculations, thus one might wonder whether the DFT can be used to obtain this value. The inaccuracy of the DFT comes from its exchange correlation functional, for example, it is represented in its absolute eigenenergy values. This V_C is the result of the electron-wave-function coupling, so as long as the wave function is described correctly, the calculated coupling constant should be reliable. We must emphasize that the two-level Hamiltonian in Eq. (9) is just a simple model to explain the connection between the anticrossing gap and the coupling constant. It is not used at all in the actual simulation.

The coupling constant V_C between E_{defect} and E_{CBM} in the other six structures are obtained in the same way and are shown in Fig. 5. It can be seen that V_C decays dramatically with the increase of the interface-defect distance, and the calculated data can be fitted well by an exponential function. On the other hand, a large fluctuation is clearly observed for the three structures with the same interface-defect distance but with a different inserted layer in between the defect and Si, indicating the important role of amorphous structure variation. We also provide a decaying curve obtained by WKB approximation in Fig. 5 to support the discussion in the following section.

IV. VALIDITY OF THE WKB APPROXIMATION

Since the WKB approximation has been frequently used to estimate the state-to-state coupling in phenomenological models, it will be helpful to compare the WKB approximation with the DFT results. According to Eq. (1), the tunneling effective mass m_t and the tunneling barrier ΔE should be obtained first. When the electric field is not considered, the tunneling barrier is just the conduction-band offset between Si and SiO$_2$, which is calculated to be 2.9 eV. The tunneling mass is taken to be $0.5m_0$ according to Ref [2]. Consequently, Eq. (1) can be rewritten as

$$V_C = \tilde{k}e^{-(d/1.62)}, \quad (11)$$
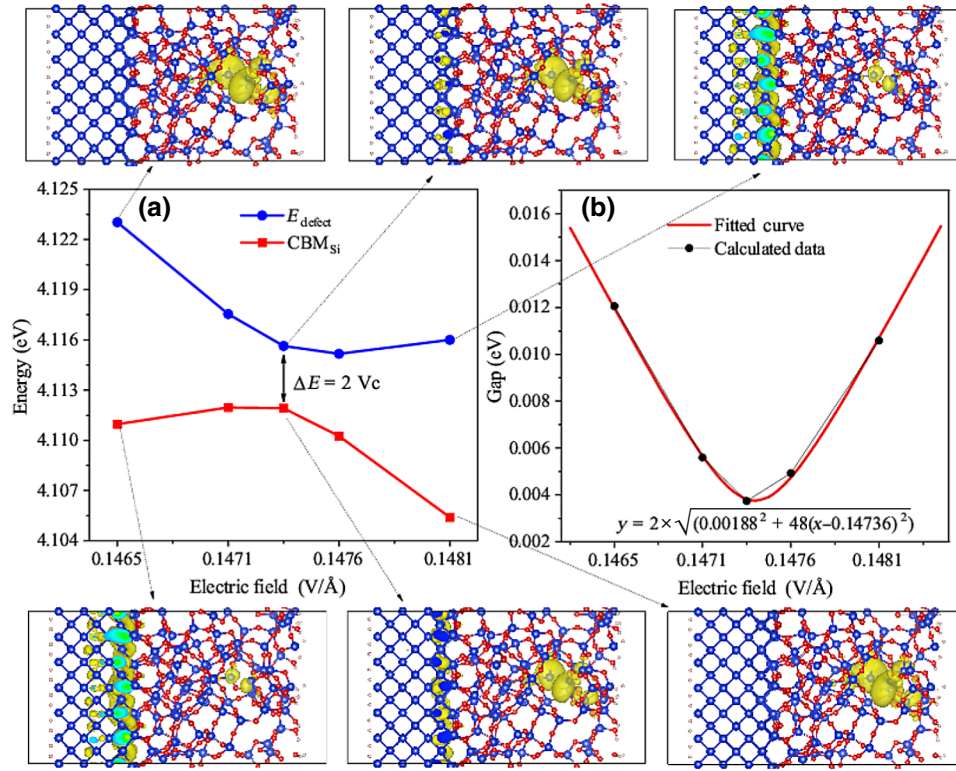
FIG. 4. The coupling process of E_{CBM} and E_{defect} driven by an electric field. (a) The changing of E_{CBM}, E_{defect}, and their wave functions with the applied electric field. (b) The fitting of the anticrossing energy gap.

where d is in units of Å. In a more sophisticated model, the electric field is used to adjust the band edge at different positions:
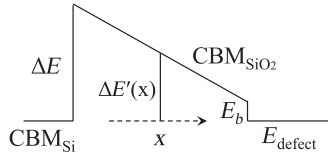
As a result, the tunneling barrier declines along the distance away from the c-Si/a-SiO$_2$ interface. Considering the case when E_{defect} is pulled down to the level of E_{CBM-Si} by the electric field, we then have

$$V_C = \tilde{k}e^{-(\sqrt{2m_t}/\hbar)\int_0^d \sqrt{[(E_b-\Delta E)/d]x+\Delta E}dx} \qquad (12)$$

where E_b is the binding energy of the defect levels inside a-SiO$_2$ or the difference between $E_{CBM}(SiO_2)$ and E_{defect}. E_b is calculated to be about 0.82 eV. Plugging in $m_t = 0.5m_0$ and $\Delta E = 2.9$ eV, we have

$$V_C = \tilde{k}e^{-(d/2.05)}, \qquad (13)$$

where d is in units of Å. Both Eqs. (11) and (13) predict an exponential decay and they are plotted in Fig. 5. As can be seen, they have much shorter decay distances (1.62 and 2.05 Å, respectively) than the one produced by *ab initio*

calculations (3.51 Å as shown in Fig. 5). One obvious way to increase the decay length in the WKB model is to use a smaller m_t. For example, if $m_t = 0.17m_0$ is used, then the second WKB model can yield a 3.51 Å decay length. This decay is inside the a-SiO$_2$, thus it is difficult to judge what effective mass one should use given the amorphous nature. Nevertheless, if c-SiO$_2$ is used instead, its effective mass is calculated to be 0.98m_0, which is obviously not able to reproduce the DFT result using the above WKB formula.

The wave function decays and their coupling inside the a-SiO$_2$ can also be observed directly from *ab initio* calculations. Here, we take the $L2$-$s1$ structure, for example, to check the coupling of the two wave functions for the case of $F = F_0$ (the exact coupling point). The reason to choose $L2$-$s1$ is that we can compare it with $L2$-$s3$ to reveal the effect of structure variation. To make the very small values visible, the wave function square (charge density) is transformed into its logarithm value and then shown in Fig. 6(a). We also manage to reduce the three-dimensional charge density distribution into one dimension by summing the values in the x-y plane, as is shown in Fig. 6(b). First, we can see from Fig. 6(a) that coupling of the two states is perhaps realized by the decays of both states from their original positions while meeting in the middle, instead of the tunneling of one state all the way to the center of the other state, which is usually the picture in the previous WKB approximation [32]. The coupling
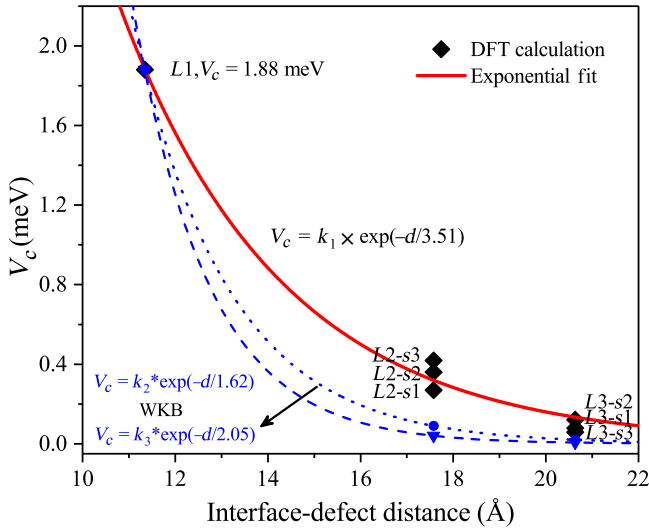
FIG. 5.   The dependence of V_C on the interface-defect distance and the structure variations. The DFT-calculated data is fitted well by an exponential curve with a decay length of 3.51 Å and a prefactor of $k_1 = 47.69$. The different DFT cases for the same c-Si–defect distance are due to different inserted a-SiO$_2$ layers between c-Si and the defect site. For comparison, the V_C decay predicted by WKB approximation with $m_t = 0.5m_0$ is also provided and the prefactors k_2 and k_3 are tuned to cross the first DFT data. It is obvious that the WKB approximation overestimates the decay rate of V_C.

FIG. 6.   The $\log(\psi_{CBM}{}^2)$ when E_{CBM} and E_{defect} couple the strongest. (a) The wave function of E_{CBM} in $L2$-$s1$. (b) The projection of charge density in $L2$-$s1$ and $L2$-$s3$ in the Z direction. The area between the two dashed lines is the inserted SiO$_2$ layer.

might happen through the whole area of their overlap. What makes it more complicated is that while the CBM state might decay as a 1D wave function, the defect state clearly decays as a three-dimensional spherical function. From Fig. 6(b), we can see that the decay of the defect state is at least two times slower than the decays of the CBM state. All these might contribute to the difference between our direct DFT-calculated results and the simple WKB-approximated results. One intriguing question is whether the left part (from the interface) and the right part (from the defect) of the wave function should be described by the same atomic characteristics. They are obviously different for the wave function inside c-Si and near the defect. There could be a coupling issue for the CBM state in c-Si to be transmitted to the defectlike state in a-SiO$_2$ region. Indeed, we see a more abrupt drop of amplitude at the interface for the CBM state, while there is a more gradual decay for the defect state in a-SiO$_2$.

To explain the V_C fluctuation in different structures, the charge-density distribution in structure $L2$-$s3$ is also shown in Fig. 6(b). It can be seen that the charge density in the two structures varies significantly around the inserted SiO$_2$ layer, and the charge density in $L2$-$s3$ is larger than that in $L2$-$s1$. This is consistent with the fact that the V_C in $L2$-$s3$ is larger than that in $L2$-$s1$, as is seen in Fig. 5. In other words, the amorphous structure in structure $L2$-$s3$ is more

favorable for the electron transfer and thus induces a larger coupling constant.

In summary, the conventional WKB approximation underestimates the electronic coupling between the E_{CBM} and E_{defect} states when only the tunneling of the CBM$_{Si}$ state is considered. It yields a too small decay length when a conventional effective mass is used for the SiO$_2$ layer. On the other hand, if $m_t = 0.17m_0$ is used, it can provide a decay curve similar to the DFT results. The DFT-calculated results also yield the prefactor $\tilde{k}$, which was unobtainable in WKB approximation, and must be calibrated by experiments [32].

V. ELECTRON TRANSFER RATES

Since E_{CBM}, E_{defect}, reorganization energy λ, and the coupling constant V_C are all obtained, the electron-trapping rate can be easily calculated using Eq. (3). Figure 7(a) shows the trapping rate at each structure when no electric filed is applied. First, it can be seen that all the trapping rates are very small, with values less than 10^{-9} s^{-1}. This is because the energy difference between E_{CBM} and E_{defect} is very large, and the resulting exponential part in Eq. (3) is very small. Second, the trapping rates of the different structures with same interface-defect distance differ greatly from each other due to the fluctuation of the coupling constant V_C and ($E_{defect}-E_{CBM}$), as is seen in Figs. 5 and 2(b). More importantly, we investigate the impact of this fluctuation due to the variations of V_C and ($E_{defect} - E_{CBM}$) separately. The variation of V_C (for the same distance defects) only changes the transition rate by a factor of three [as demonstrated by the maximum transition rate
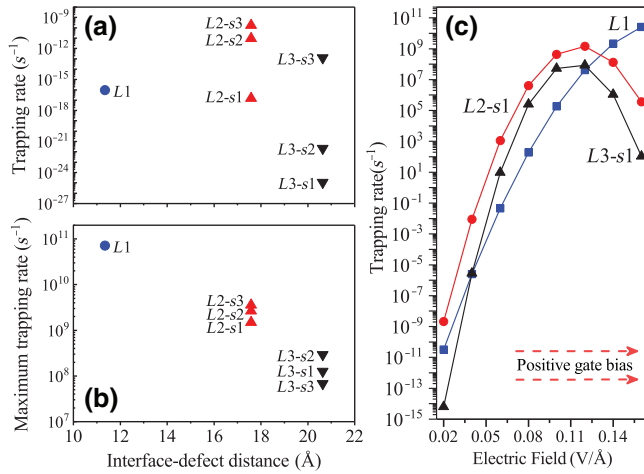
FIG. 7. The electron-trapping rate from E_{CBM} to E_{defect}. (a) The trapping rate in different structures when no electric field is applied. (b) The maximum trapping rate in different structures under the critical electric field F_0. (c) The dependence of the trapping rate on electric fields.

in Fig. 7(b)], but the change caused by the variation in ($E_{defect}-E_{CBM}$) can be as much as 10 orders of magnitude as shown in Fig. 7(a).

However, the above-zero-electric-field transition is of minimum consequence. What is more important is the transition under an applied electric field (when the gate is turned on), especially when the defect level is in resonance with the Si CBM level due to the electric field. We thus calculate the transition rate as a function of the applied electric field. Denoting the distance between defects and the Si/SiO$_2$ interface as $d_{I\text{-}D}$, and the electric field in the oxide induced by a positive gate voltage of F_{ox}, the Eq. (7) will be rewritten as

$$\Delta G = E_{defect} - d_{I\text{-}D}F_{ox} - E_{CBM}$$
$$- \lambda_{defect} + \lambda_{CBM\text{-}Si}. \qquad (14)$$

Combining Eqs. (3) and (14), it can be seen that the charge-trapping rate rises when E_{defect} approaches E_{CBM} (of silicon), and it falls when E_{defect} departs from E_{CBM} under a very large electric field. Taking structures $L1$, $L2\text{-}s1$, and $L3\text{-}s1$, for example, we calculate the oxide-electric-field-dependent trapping rates. As is seen in Fig. 7(c), the trapping rate grows very fast with the enhancing of the electric field at the beginning, but it starts to decrease after reaching a critical electric field. The defect in structure $L1$ is closest to the Si/SiO$_2$ interface, and thus its trapping rate changes slowest with the electric field. The maximum trapping rates in all structures are shown in Fig. 7(b). This transfer rate clearly decays with $d_{I\text{-}D}$ just as the V_C does. In other words, the maximum electron-trapping rate from CBM to defect is controlled by V_C.

VI. CONCLUSION

In conclusion, we investigate the electron-trapping process in c-Si/a-SiO$_2$ interface structures by using the HSE-hybrid-functional-based DFT calculation and the Marcus electron transfer theory. The effect of interface-defect distance and amorphous structure variation are both systematically considered and the validity and accuracy of the WKB approximation are evaluated. Results show that the coupling constant between the silicon CBM state and oxygen-vacancy-defect state decays exponentially with the increase of the interface-defect distance. However, the conventional WKB model with the commonly used parameters significantly underestimates the decay length. There are fluctuations in the coupling constant due to both the different local environment at the defect and to different amorphous structures in the region between the defect and the c-Si. This structural randomness caused fluctuation in the coupling constant can be up to 50% of its amplitude (for the same $d_{I\text{-}D}$). The calculation of the coupling constant by DFT provides a way to calibrate the critical parameters used in phenomenological device simulation models. Finally, the electron-trapping rate from Si to oxygen-vacancy defect is found to be mainly controlled by the energy difference ($E_{defect}-E_{CBM}$) if no voltage bias is applied. However, it is controlled by the coupling constant when E_{defect} approaches E_{CBM} under positive gate voltages. The electron-trapping rates from c-Si to the O_V defect level at such a resonant gate voltage are 10^{11} s^{-1}, and 10^8 s^{-1} when the c-Si–defect distance is 10 and 20 Å, respectively.

[1] S. Mahapatra, N. Goel, S. Desai, S. Gupta, B. Jose, S. Mukhopadhyay, K. Joshi, A. Jain, A. E. Islam, and M. A. Alam, A comparative study of different physics-based NBTI Models, IEEE Trans. Electron Devices **60**, 901 (2013).

[2] T. Grasser, B. Kaczer, W. Goes, Th. Aichinger, Ph. Hehenberger, and M. Nelhiebel, in *Proc. Int. Rel. Phys. Symp.* (2009), pp. 33–44.

[3] N. Parihar, U. Sharma, S. Mukhopadhyay, N. Goel, A. Chaudhary, R. Rao, and S. Mahapatra, in *Proc. Int. Rel. Phys. Symp.* (2017), pp. XT-1.1–XT-1.11.

[4] J. H. Lee, W. H. Wu, A. E. Islam, M. A. Alam, and A. S. Oates, in *Proc. Int. Rel. Phys. Symp.*, 745 (2008), pp. 745–746.

[5] V. Huard, in *Proc. Int. Rel. Phys. Symp.* (2010), pp. 33–42.

[6] L. Tsetseris, X. J. Zhou, D. M. Fleetwood, R. D. Schrimpf, and S. T. Pantelides, Physical mechanisms of negative-bias temperature instability, Appl. Phys. Lett. **86**, 142103 (2005).

[7] D. K. Schroder and J. A. Babcock, Negative bias temperature instability: Road to cross in deep submicron silicon semiconductor manufacturing, J. Appl. Phys. **94**, 1 (2003).

[8] D. M. Fleetwood, P. S. Winokur, R. A. Reber, T. L. Meisenheimer, J. R. Schwank, M. R. Shaneyfelt, and L. C. Riewe, Effects of oxide traps, interface traps, and "border traps" on metal-oxidesemiconductor devices, J. Appl. Phys. **73**, 5058 (1993).

[9] M. Denais, V. Huard, C. Parthasarathy, G. Ribes, F. Perrier, N. Revil, and A. Bravaix, Interface trap generation and hole trapping under NBTI and PBTI in advanced CMOS technology with a 2-nm gate oxide, IEEE Trans. Device Mater. Rel. **4**, 715 (2004).

[10] J. H. Stathis and S. Zafar, The negative bias temperature instability in MOS devices: A review, Microelectron. Reliab. **46**, 270 (2006).

[11] K. O. Jeppson and C. M. Svensson, Negative bias stress of MOS devices at high electric fields and degradation of MNOS devices, J. Appl. Phys. **48**, 2004 (1977).

[12] S. Ogawa and N. Shiono, Generalized diffusion-reaction model for the low-field charge-buildup instability at the Si-SiO_2 interface, Phys. Rev. B **51**, 4218 (1995).

[13] M. Houssa, M. Aoulaiche, S. De Gendt, G. Groeseneken, M. M. Heyns, and A. Stesmans, Reaction-dispersive proton transport model for negative bias temperature instabilities, Appl. Phys. Lett. **86**, 093506 (2005).

[14] V. Huard, M. Denais, and C. Parthasarathy, NBTI degradation: From physical mechanisms to modelling, Microelectron. Reliab. **46**, 1 (2006).

[15] H. Reisinger, O. Blank, W. Heinrigs, A. Mühlhoff, W. Gustin, and C. Schlünder, in *Proc. IRPS* (2006), pp. 448–453.

[16] T. Grasser, W. Goes, V. Sverdlov, and B. Kaczer, in *Proc. IRPS*, 268 (2007), pp. 268–280.

[17] B. Kaczer, T. Grasser, P. J. Roussel, J. Martin-Martinez, R. O'Connor, B. J. O'Sullivan, and G. Groeseneken, in *Proc. IRPS* (2008), pp. 20–27.

[18] T. Grasser, B. Kaczer, W. Goes, H. Reisinger, T. Aichinger, P. Hehenberger, P. Wagner, F. Schanovsky, J. Franco, M. T. Luque, and M. Nelhiebel, The paradigm shift in understanding the bias temperature instability: From reaction–diffusion to switching oxide traps, IEEE Trans. Electron Devices **58**, 3652 (2011).

[19] G. Rzepa, J. Franco, B. O'Sullivan, A. Subirats, M. Simicic, G. Hellings, P. Weckx, M. Jech, T. Knobloch, M. Waltl, P. J. Roussel, D. Linten, B. Kaczer, and T. Grasser, Comphy — A compact-physics framework for unified modeling of BTI, Microelectron. Reliab. **85**, 49 (2018).

[20] T. Grasser, B. Kaczer, W. Goes, Th. Aichinger, Ph. Hehenberger, and M. Nelhiebel, Understanding negative bias temperature instability in the context of hole trapping, Microelectron. Eng. **86**, 1876 (2009).

[21] Z. Q. Teo, D. S. Ang, and K. S. See, in *IEDM Tech. Dig.* (2009), pp. 737–740.

[22] B. Kaczer, T. Grasser, P. J. Roussel, J. Franco, R. Degraeve, L. A. Ragnarsson, E. Simoen, G. Groeseneken, and H. Reisinger, in *Proc. IRPS* (2010), pp. 26–32.

[23] T. Grasser, Stochastic charge trapping in oxides: From random telegraph noise to bias temperature instabilities, Microelectron. Reliab. **52**, 39 (2012).

[24] N. L. Anderson, R. P. Vedula, P. A. Schultz, R. M. Van Ginhoven, and A. Strachan, First-Principles Investigation of Low Energy E' Center Precursors in Amorphous Silica, Phys. Rev. Lett. **106**, 206402 (2011).

[25] C. L. Kuo and G. S. Hwang, Structure and Interconversion of Oxygen-Vacancy-Related Defects on Amorphous Silica, Phys. Rev. Lett. **97**, 066101 (2006).

[26] A. M. El-Sayed, M. B. Watkins, T. Grasser, V. V. Afanas'ev, and A. L. Shluger, Hydrogen-Induced Rupture of Strained Si-O Bonds in Amorphous Silicon Dioxide, Phys. Rev. Lett. **114**, 115503 (2015).

[27] A. M. El-Sayed, Y. Wimmer, W. Goes, T. Grasser, V. V. Afanas'ev, and A. L. Shluger, Theoretical models of hydrogen-induced defects in amorphous silicon dioxide, Phys. Rev. B **92**, 014107 (2015).

[28] A. M. El-Sayed, M. B. Watkins, V. V. Afanas'ev, and A. L. Shluger, Nature of intrinsic and extrinsic electron trapping in SiO_2, Phys. Rev. B **89**, 125201 (2014).

[29] F. Cerbu, O. Madia, D. V. Andreev, S. Fadida, M. Eizenberg, L. Breuil, J. G. Lisoni, J. A. Kittl, J. Strand, A. L. Shluger, V. V. Afanas'ev, M. Houssa, and A. Stesmans, Intrinsic electron traps in atomic-layer deposited HfO_2 insulators, Appl. Phys. Lett. **108**, 222901 (2016).

[30] E. Mehes and C. H. Patterson, Defects at the $Si(001)/a$-SiO_2 interface: Analysis of structures generated with classical force fields and density functional theory, Phys. Rev. Mater. **1**, 044602 (2017).

[31] F. Zheng, H. H. Pham, and L.-W. Wang, Effects of the c-Si/a-SiO_2 interfacial atomic structure on its band alignment: an ab initio study, Phys. Chem. Chem. Phys. **19**, 32617 (2017).

[32] W. Goes, Y. Wimmer, A.-M. El-Sayed, G. Rzepa, M. Jech, A. L. Shluger, and T. Grasser, Identification of oxide defects in semiconductor devices: A systematic approach linking DFT to rate equations and experimental evidence, Microelectron. Reliab. **87**, 286 (2018).

[33] S. Makram-Ebeid and M. Lannoo, Quantum model for phonon-assisted tunnel ionization of deep levels in a semiconductor, Phys. Rev. B **25**, 6406 (1982).

[34] A. C. T. van Duin, A. Strachan, S. Stewman, Q. Zhang, X. Xu, and W. A. Goddard, ReaxFF$_{SiO}$ reactive force field for silicon and silicon oxide systems, J. Phys. Chem. A **107**, 3803 (2003).

[35] W. Jia, Z. Cao, L. Wang, J. Fu, X. Chi, W. Gao, and L. W. Wang, The analysis of a plane wave pseudopotential density functional theory code on a GPU machine, Comput. Phys. Commun. **184**, 9 (2013).

[36] W. Jia, J. Fu, Z. Cao, L. Wang, X. Chi, W. Gao, and L. W. Wang, Fast plane wave density functional theory molecular dynamics calculations on multi-GPU machines, J. Comput. Phys. **251**, 102 (2013).

[37] R. A. Marcus, On the Theory of Oxidation-Reduction Reactions Involving Electron Transfer. I, J. Chem. Phys. **24**, 966 (1956).

[38] R. A. Marcus, On the theory of electron-transfer reactions. VI. Unified treatment for homogeneous and electrode reactions, J. Chem. Phys. **43**, 679 (1965).

[39] K. Tarafder, Y. Surendranath, J. H. Olshansky, A. P. Alivisatos, and L. W. Wang, Hole transfer dynamics from a CdSe/CdS quantum rod to a tethered ferrocene derivative, J. Am. Chem. Soc. **136**, 5121 (2014).

[40] H. Wei, J. W. Luo, S. S. Li, and L. W. Wang, Revealing the origin of fast electron transfer in TiO_2-based dye-sensitized solar cells, J. Am. Chem. Soc. **138**, 8165 (2016).

[41] I. H. Chu, M. Radulaski, N. Vukmirovic, H. P. Cheng, and L. W. Wang, Charge transport in a quantum dot supercrystal, J. Phys. Chem. C **115**, 21409 (2011).

[42] L. Shi, K. Xu, and L. W. Wang, Comparative study of ab initio nonradiative recombination rate calculations under different formalisms, Phys. Rev. B **91**, 205315 (2015).

[43] A. Alkauskas, Q. Yan, and C. G. Van de Walle, First-principles theory of nonradiative carrier capture via multiphonon emission, Phys. Rev. B **90**, 075202 (2014).

[44] G. D. Barmparis, Y. S. Puzyrev, X.-G. Zhang, and S. T. Pantelides, Theory of inelastic multiphonon scattering and carrier capture by defects in semiconductors: Application to capture cross sections, Phys. Rev. B **92**, 214111 (2015).

[45] See Supplemental Material at http://link.aps.org/supplemental/10.1103/PhysRevApplied.11.044058 for S1 the validity of single k point, S2 "anti-crossing" and "coupling constant", S3 the advantage of our method in reducing the influence of image electrostatic interaction, and S4 size effect.

[46] A. M. El-Sayed, Doctoral dissertation, University College London, 2015.

[47] V. Coropceanu, J. Cornil, D. A. da S. Filho, Y. Olivier, R. Silbey, and J.-L. Brédas, Charge transport in organic semiconductors, Chem. Rev. **107**, 926 (2007).

[48] C. Cohen-Tannoudji, B. Diu, and F. Laloë, *Quantum Mechanics* (Wiley, New-York, 1991), Vol. 1, p. 409.